Computers and Mathematics with Applications 62 (2011) 737–745

Contents lists available at ScienceDirect

Computers and Mathematics with Applications

journal homepage: www.elsevier.com/locate/camwa

Multiphase image segmentation using a phase-field model

Yibao Li, Junseok Kim *

Department of Mathematics, Korea University, Seoul 136-701, Republic of Korea

ARTICLE INFO

Article history:
Received 12 November 2010
Received in revised form 12 May 2011
Accepted 31 May 2011

Keywords:
Image segmentation
Modica-Mortola
Allen–Cahn equation
Phase-field method

ABSTRACT

In this paper, we propose a new, fast, and stable hybrid numerical method for multiphase image segmentation using a phase-field model. The proposed model is based on the Allen–Cahn equation with a multiple well potential and a data-fitting term. The model is computationally superior to the previous multiphase image segmentation via Modica-Mortola phase transition and a fitting term. We split its numerical solution algorithm into linear and a nonlinear equations. The linear equation is discretized using an implicit scheme and the resulting discrete system of equations is solved by a fast numerical method such as a multigrid method. The nonlinear equation is solved analytically due to the availability of a closed-form solution. We also propose an initialization algorithm based on the target objects for the fast image segmentation. Finally, various numerical experiments on real and synthetic images with noises are presented to demonstrate the efficiency and robustness of the proposed model and the numerical method.

1. Introduction

Image segmentation is one of the fundamental tasks in image processing and computer vision. It forms a crucial preliminary step for subsequent object recognition and interpretation [1]. Its goal is to partition a given image into regions that contain distinct objects. The most common form of segmentation is based on the assumption that distinct objects in an image have different and approximately constant colors. A natural approach is therefore to decompose an image domain into approximately homogeneous regions that are separated by sharp changes in image features.

Recently, many research papers have been published on methods of multiphase image segmentation [2–12]. For example, Chan and Vese (CV) [3] proposed a multiphase level-set framework for image segmentation using the Mumford and Shah model for piecewise constant and piecewise smooth optimal approximations. Their model can segment 2^K phases of the image with K level-set functions. Thus, the multiphase CV model evolves more regions than necessary whenever the number of regions is not a power of two. Samson et al. [10] partitioned K phases using K level-set functions for multiphase image classification. Lie et al. [7] proposed a variant of the level-set formulation for multiphase image segmentation by introducing a piecewise constant level-set function and using each constant value to represent a unique phase. In [6], Jung et al. proposed a phase-field method to solve the multiphase piecewise constant segmentation problem. The method is based on the phase transition model of Modica and Mortola with a sinusoidal potential and a fitting term. It is a variational partial differential equation approach that is closely connected to the Mumford–Shah model.

The objective of this paper is to propose a new, fast, and stable hybrid numerical method for multiphase image segmentation using a phase-field model which is based on the Allen–Cahn (AC) equation [13] with a multiple well potential and a data-fitting term. We employ the recently developed hybrid operator splitting method for the AC equation [14]. We split its numerical solution algorithm into a linear diffusion equation with a source term and a nonlinear equation. The linear

* Corresponding author. Tel.: +82 2 3290 3077; fax: +82 2 929 8562.
E-mail address: cfdkim@korea.ac.kr (J. Kim).
URL: http://math.korea.ac.kr/~cfdkim/ (J. Kim).

0898-1221/$ – see front matter © 2011 Elsevier Ltd. All rights reserved.
doi:10.1016/j.camwa.2011.05.054

equation is discretized using an implicit scheme and the resulting discrete system of equations is solved by a multigrid method. The nonlinear equation is solved using a closed-form solution. We also propose an initialization algorithm based on the target objects for the fast and robust multiphase image segmentation.

This paper is organized as follows. In Section 2, the proposed model for multiphase image segmentation is given. In Section 3, we describe the proposed an almost unconditionally stable hybrid operator splitting method. In Section 4, we perform some characteristic numerical experiments for multiphase image segmentation to demonstrate the efficiency and robustness of the proposed model and the numerical method. Finally, conclusions are given in Section 5.

2. Description of the proposed model

A phase-field model is a mathematical model for solving interfacial problems. It has been applied to many applications such as spinodal decomposition [15], dendritic crystal growth [16–19], vesicle membranes [20], image segmentation [21], motion by mean curvature [22], and multiphase fluid flows [23–28]. In a phase-field model, the phase-field or order parameter is introduced to distinguish one phase from the other. This phase-field takes distinct values (for instance 0 and 1 for a binary system) in each of the phases with a smooth transition between both values. Interfaces are identified by the variation or specific level set of the phase-field.

Since we are interested in multiphase image segmentation using the Allen–Cahn equation with a multiple well potential and a data-fitting term, we now briefly review the following AC equation with a double well potential on a domain $\Omega \subset \mathbf{R}^d$ $(d = 1, 2, 3)$:

$$\frac{\partial \phi(\mathbf{x}, t)}{\partial t} = -M(F'(\phi(\mathbf{x}, t)) - \epsilon^2 \Delta \phi(\mathbf{x}, t)), \quad \mathbf{x} \in \Omega,\ 0 < t \le T, \tag{1}$$

where the quantity $\phi(\mathbf{x}, t)$ is defined to be the difference between the concentrations of the two mixtures' components, the parameter M is a positive constant mobility, the function $F(\phi)$ is the Helmholtz free-energy density, and the small constant ϵ is the gradient energy parameter related to the interfacial energy. A double well form, i.e., $F(\phi) = 0.25\phi^2(\phi - 1)^2$ is typically chosen. The boundary condition is

$$\frac{\partial \phi}{\partial \mathbf{n}} = 0 \quad \text{on } \partial\Omega, \tag{2}$$

where $\frac{\partial}{\partial \mathbf{n}}$ denotes the normal derivative on $\partial\Omega$. The physical meaning of the condition is that the total free energy of the mixture decreases in time. The Allen–Cahn equation [13] was originally introduced as a phenomenological model for anti-phase domain coarsening in a binary alloy. It has been applied to a wide range of problems such as phase transitions, image analysis, the motion by mean curvature flows, and crystal growth. The AC equation arises from the Ginzburg–Landau free energy,

$$\mathcal{E}(\phi) := \int_\Omega \left(F(\phi) + \frac{\epsilon^2}{2} |\nabla \phi|^2 \right) \mathrm{d}\mathbf{x}. \tag{3}$$

The AC equation is the L^2-gradient flow of the total free energy $\mathcal{E}(\phi)$. We differentiate the energy $\mathcal{E}(\phi)$ to get

$$\begin{aligned} \frac{\mathrm{d}}{\mathrm{d}t}\mathcal{E}(\phi) &= \int_\Omega (F'(\phi)\phi_t + \epsilon^2 \nabla\phi \cdot \nabla\phi_t)\mathrm{d}\mathbf{x} \\ &= \int_\Omega (F'(\phi) - \epsilon^2 \Delta\phi)\phi_t \mathrm{d}\mathbf{x} = -M \int_\Omega (\phi_t)^2 \mathrm{d}\mathbf{x} \le 0, \end{aligned} \tag{4}$$

where we have used an integration by parts and the boundary condition (2). Therefore, the total energy is non-increasing in time; that is, the total energy is a Lyapunov functional for solutions of the AC equation. Now, we review a derivation of the AC equation as a gradient flow [29,30]. It is natural to seek a law of evolution in the form

$$\frac{\partial \phi}{\partial t} = -M \,\mathrm{grad}\, \mathcal{E}(\phi). \tag{5}$$

The symbol "grad" here denotes the gradient on the manifold in $L^2(\Omega)$ space. Let the domain of definition for the functional $\mathcal{E}$ be $\mathcal{D} = \left\{ \phi \in H^2(\Omega) \middle| \frac{\partial \phi}{\partial \mathbf{n}} = 0 \text{ on } \partial\Omega \right\}$. Let $\phi, \psi \in \mathcal{D}$. Then, we have

$$\begin{aligned} (\mathrm{grad}\, \mathcal{E}(\phi), \psi)_{L^2} &= \left. \frac{\mathrm{d}}{\mathrm{d}\theta} \mathcal{E}(\phi + \theta\psi) \right|_{\theta=0} = \lim_{\theta \to 0} \frac{1}{\theta} (\mathcal{E}(\phi + \theta\psi) - \mathcal{E}(\phi)) \\ &= \int_\Omega (F'(\phi) - \epsilon^2 \Delta\phi)\psi \mathrm{d}\mathbf{x} = (F'(\phi) - \epsilon^2 \Delta\phi, \psi)_{L^2}, \end{aligned}$$

where we have used an integration by parts and the boundary condition (2). We identify $\mathrm{grad}\mathcal{E}(\phi) \equiv F'(\phi) - \epsilon^2 \Delta\phi$, then Eq. (5) becomes the AC equation [29].

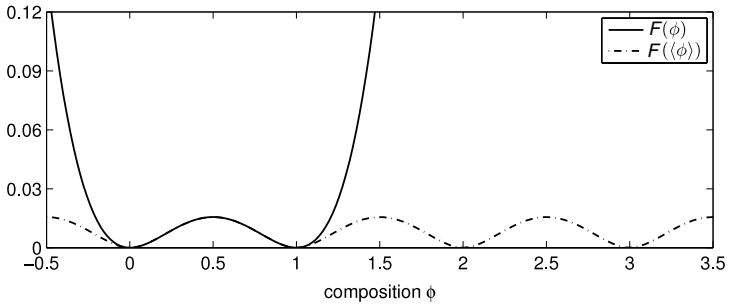

Fig. 1. A double well potential, $F(\phi) = 0.25\phi^2(\phi - 1)^2$ and a periodic potential, $F(\langle\phi\rangle) = 0.25\langle\phi\rangle^2(\langle\phi\rangle - 1)^2$.

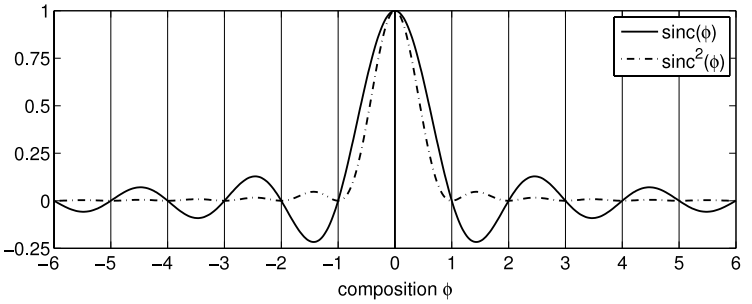

Fig. 2. $\mathrm{sinc}(\phi) = \sin(\pi\phi)/(\pi\phi)$ and $\mathrm{sinc}^2(\phi)$.

Next, we extend this two-phase Allen–Cahn model into a multiphase Allen–Cahn model with a data-fitting term. A multiphase-field approximation ($K + 1$ phase fields) for minimizing the Mumford–Shah functional is given by the following energy functional:

$$\mathcal{E}(\phi) = \int_\Omega \left(\frac{F(\langle\phi\rangle)}{\varepsilon^2} + \frac{|\nabla\phi|^2}{2} + G_K(\phi, f_0) \right) \mathrm{d}\mathbf{x}. \tag{6}$$

Here $\langle\phi\rangle = \phi - [\phi]$, where $[\phi]$ is the largest integer not greater than ϕ. The first term $F(\langle\phi\rangle)$ in the energy functional is a periodic potential as shown in Fig. 1. This term derives the phase-field variable ϕ to the closest integer values, which will be regions of approximately piecewise-constant intensities. The second term makes the transition between phase levels smooth and penalizes high oscillations of the phase-field. The third term in the functional is a fitting term written in terms of ϕ and is defined as

$$G_K(\phi, f_0) = \frac{\lambda}{2} \sum_{k=0}^{K} (C_k - f_0)^2 \mathrm{sinc}^2(\phi - k),$$

where λ is a nonnegative parameter, f_0 is the given image, and C_k is the average of f_0 in the k-level ($k = 0, 1, \ldots, K$), i.e.,

$$C_k = \frac{\int_\Omega f_0(\mathbf{x}) \mathrm{sinc}^2(\phi(\mathbf{x}) - k)\mathrm{d}\mathbf{x}}{\int_\Omega \mathrm{sinc}^2(\phi(\mathbf{x}) - k)\mathrm{d}\mathbf{x}}.$$

Functions $\mathrm{sinc}(\phi) = \sin(\pi\phi)/(\pi\phi)$ and $\mathrm{sinc}^2(\phi)$ are shown in Fig. 2.

We note that our model is similar to that of Jung et al. [6] except that they used a sinusoidal function while we use a periodic quartic polynomial as a potential. By using the polynomial potential, we can derive a very efficient and accurate numerical scheme based on an operator splitting technique. For a governing equation, we apply Eq. (5) and get the following gradient descent flow equation:

$$\phi_t = -\frac{F'(\langle\phi\rangle)}{\varepsilon^2} + \Delta\phi - \lambda \sum_{k=0}^{K} (C_k - f_0)^2 \left(\frac{\sin(2\pi(\phi - k))}{\pi(\phi - k)^2} - \frac{2\sin^2(\pi(\phi - k))}{\pi^2(\phi - k)^3} \right). \tag{7}$$

3. Description of the numerical algorithms

We shall discretize the governing equation (7) in two-dimensional space, i.e., $\Omega = (a, b) \times (c, d)$. Let N_x and N_y be positive even integers, $h = (b - a)/N_x$ be the uniform mesh size, and $\Omega_h = \{(x_i, y_j) : x_i = (i - 0.5)h, y_j = (j - 0.5)h, 1 \leq$

$i \le N_x,\ 1 \le j \le N_y\}$ be the set of cell-centers. Let ϕ_{ij}^n be approximations of $\phi(x_i, y_j, n\Delta t)$, where $\Delta t = T/N_t$ is the time step, T is the final time, and N_t is the total number of time steps. Then we propose the following operator splitting numerical algorithm of the proposed model.

$$\frac{\phi^{n+1}-\phi^n}{\Delta t} = -\frac{F'(\langle\phi^{n+1}\rangle)}{\epsilon^2} + \Delta_d\phi^{n+\frac{1}{2}} - \lambda\sum_{k=0}^{K}(C_k^n - f_0)^2 \times \left(\frac{(\phi^n-k)^2\sin(2\pi(\phi^n-k)) - 2(\phi^n-k)\sin^2(\pi(\phi^n-k))}{\pi^2(\phi^n-k)^4+\delta}\right), \tag{8}$$

where we added a small value δ in the denominator to avoid singularities and C_k^n is defined as following

$$C_k^n = \sum_i^{N_x}\sum_j^{N_y} f_{0,ij}\,\mathrm{sinc}^2(\phi_{ij}-k) \Big/ \sum_i^{N_x}\sum_j^{N_y}\mathrm{sinc}^2(\phi_{ij}-k),$$

here $\mathrm{sinc}^2(\phi) = (\sin^2(\pi\phi)+\delta)/(\pi^2\phi^2+\delta)$.

We take the following two steps:

$$\frac{\phi^{n+\frac{1}{2}}-\phi^n}{\Delta t} = \Delta_d\phi^{n+\frac{1}{2}} - \lambda\sum_{k=0}^{K}(C_k^n - f_0)^2\left(\frac{(\phi^n-k)^2\sin(2\pi(\phi^n-k)) - 2(\phi^n-k)\sin^2(\pi(\phi^n-k))}{\pi^2(\phi^n-k)^4+\delta}\right) \tag{9}$$

and

$$\frac{\phi^{n+1}-\phi^{n+\frac{1}{2}}}{\Delta t} = -\frac{F'(\langle\phi^{n+1}\rangle)}{\epsilon^2}. \tag{10}$$

We solve Eq. (9) by a multigrid method [31,32]. We can consider Eq. (10) as an implicit scheme for the following Eq. (11) with the initial condition $\phi^{n+\frac{1}{2}}$.

$$\phi_t = -\frac{F'(\langle\phi\rangle)}{\epsilon^2}. \tag{11}$$

The solution at $t = \Delta t$ of Eq. (11) is obtained by the method of separation of variables [33] and is given as

$$\langle\phi^{n+1}\rangle = 0.5 + \frac{\langle\phi^{n+\frac{1}{2}}\rangle - 0.5}{\sqrt{\mathrm{e}^{\frac{-\Delta t}{2\epsilon^2}} + (2\langle\phi^{n+\frac{1}{2}}\rangle - 1)^2(1-\mathrm{e}^{\frac{-\Delta t}{2\epsilon^2}})}}.$$

Hence, the solution of Eq. (10) is

$$\phi^{n+1} = 0.5 + \frac{\langle\phi^{n+\frac{1}{2}}\rangle - 0.5}{\sqrt{\mathrm{e}^{\frac{-\Delta t}{2\epsilon^2}} + (2\langle\phi^{n+\frac{1}{2}}\rangle - 1)^2(1-\mathrm{e}^{\frac{-\Delta t}{2\epsilon^2}})}} + [\phi^{n+\frac{1}{2}}]. \tag{12}$$

Finally, our proposed scheme is written as

$$\frac{\phi^{n+\frac{1}{2}}-\phi^n}{\Delta t} = \Delta_d\phi^{n+\frac{1}{2}} - \lambda\sum_{k=0}^{K}(C_k^n - f_0)^2\left(\frac{(\phi^n-k)^2\sin(2\pi(\phi^n-k)) - 2(\phi^n-k)\sin^2(\pi(\phi^n-k))}{\pi^2(\phi^n-k)^4+\delta}\right), \tag{13}$$

$$\phi^{n+1} = 0.5 + \frac{\langle\phi^{n+\frac{1}{2}}\rangle - 0.5}{\sqrt{\mathrm{e}^{\frac{-\Delta t}{2\epsilon^2}} + (2\langle\phi^{n+\frac{1}{2}}\rangle - 1)^2(1-\mathrm{e}^{\frac{-\Delta t}{2\epsilon^2}})}} + [\phi^{n+\frac{1}{2}}]. \tag{14}$$

The homogeneous Neumann boundary condition is applied to the domain. However, it is not restricted to the Neumann condition, we can use other boundary conditions such as periodic, Dirichlet, and combinations of these. We note that the first Eq. (13) is the discrete implicit diffusion equation with a source term. The second Eq. (14) is the analytic solution for the ordinary differential equation.

4. Numerical experiments

In this section, we tested our proposed model and its computational algorithm on generic numerical experiments such as piecewise constant images with and without noises, landscape image, and MR images.

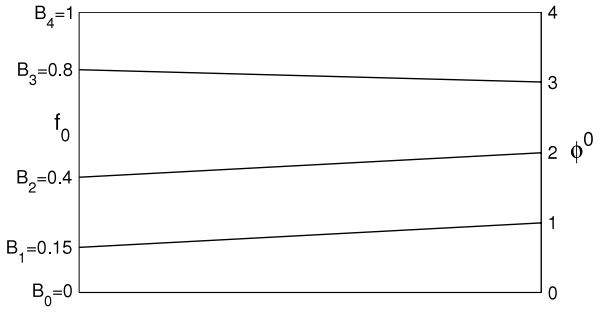

Fig. 3. Proposed initialization.

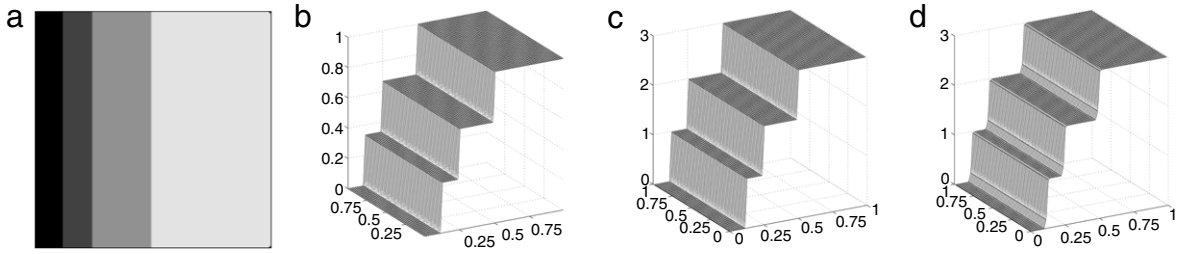

Fig. 4. Multiphase image with uniform heights. The size of the image is 128 × 128. (a) Original image f_0, (b) the value of original image f_0, (c) initial phase-field ϕ^0, and (d) converged phase-field ϕ after 4 iterations.

4.1. Proposed initialization

Regarding the initial guess for the phase-field ϕ, authors in [6] have typically adopted random solution values between -0.5 and $K + 0.5$ for simple images. In our numerical experiments, we normalize a given image f as $f_0 = \frac{f - f_{\min}}{f_{\max} - f_{\min}}$, where $f_{\max}$ and $f_{\min}$ are the maximum and the minimum values of the given image, respectively. Across the interfacial regions, the concentration field varies from 0.1 to 0.9 over a distance of approximately $4\sqrt{2}\epsilon \tanh^{-1}(0.9)$. Therefore, if we want this value to be approximately m grid points, the ϵ value needs to be taken as follows: $\epsilon_m = hm/[4\sqrt{2}\tanh^{-1}(0.9)]$. In this paper, we used ϵ_2, ϵ_3, and ϵ_5 depending on test images and mesh sizes. We found that the results with different ϵ_m values make little differences. Note that we use the same computational domain $\Omega = (0, 1) \times (0, 1)$ throughout the paper. We will give the CPU time, in seconds, of our calculations, performed on a 3 GHz with 3 GB of RAM.

For the initial profile we propose the following:

$$\phi_{ij}^0 = k - 1 + \frac{f_{0,ij} - B_{k-1}}{B_k - B_{k-1}} \text{ if } f_{0,ij} \in [B_{k-1}, B_k] \quad \text{for } k = 1, \ldots, K, \tag{15}$$

where B_k for $k = 0, \ldots, K$ are target levels of the image. For example, if we have five target values, $B_0 = 0$, $B_1 = 0.15$, $B_2 = 0.4$, $B_3 = 0.8$, $B_4 = 1$, then we have the initial phase-field according to Eq. (15) and this procedure is illustrated in Fig. 3.

Fig. 4 shows a simple synthetic image that contains four levels of colors. (a) and (b) are the original image and the value of original image f_0, respectively. (c) is the initial phase-field ϕ^0. (d) shows the converged phase-field after 4 iterations. It took 0.219 s CPU. The parameters used in the experiment are ϵ_3, $\Delta t = 5\text{E} - 6$, $h = 1/128$, $\lambda = 10$, and target values $B_0 = 0$, $B_1 = 0.3333$, $B_2 = 0.6667$, and $B_3 = 1$.

Next, we set nonuniform heights with 0, 0.1, 0.2, and 1 as shown in Fig. 5(a) and (b). Fig. 5(c) and (d) are the initial profile and converged solution with 4 iterations and 0.219 s CPU. Here we used the same parameters as the previous test with $B_0 = 0$, $B_1 = 0.1026$, $B_2 = 0.2003$, and $B_3 = 1.0$. We can confirm that the new initialization also works well with nonuniform heights.

4.2. Complex synthetic image

The next example is taken from [6]. Fig. 6(a) shows a complex synthetic image with multiple objects and several generic visual structures. The interface parameter ϵ_5, time step $\Delta t = 5\text{E} - 6$, $h = 1/256$, and $\lambda = 10$ are used with the initial value $B_0 = 0$, $B_1 = 0.2471$, $B_2 = 0.4980$, $B_3 = 0.7529$, and $B_4 = 1$. Fig. 6(b)–(f) show the filled contours for each level from $k = 0$ to $k = 4$. White regions are segmented areas. It took 2 iterations and 0.625 s CPU time, while the previous model in [6] took 18 iterations and 37.109 s CPU time.

In many real applications the number of levels to detect is not known a priori. Therefore, a robust and reliable algorithm should find the correct segmentation even when the exact number of phases is not known. To confirm that our algorithm can

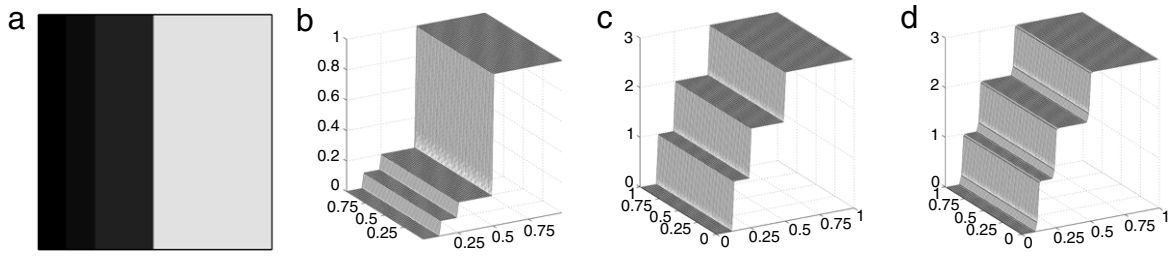

Fig. 5. Multiphase image with nonuniform heights. (a) Original image f_0 with image size 128×128, (b) the value of original image f_0, (c) initial phase-field ϕ^0, and (d) converged phase-field ϕ after 4 iterations.

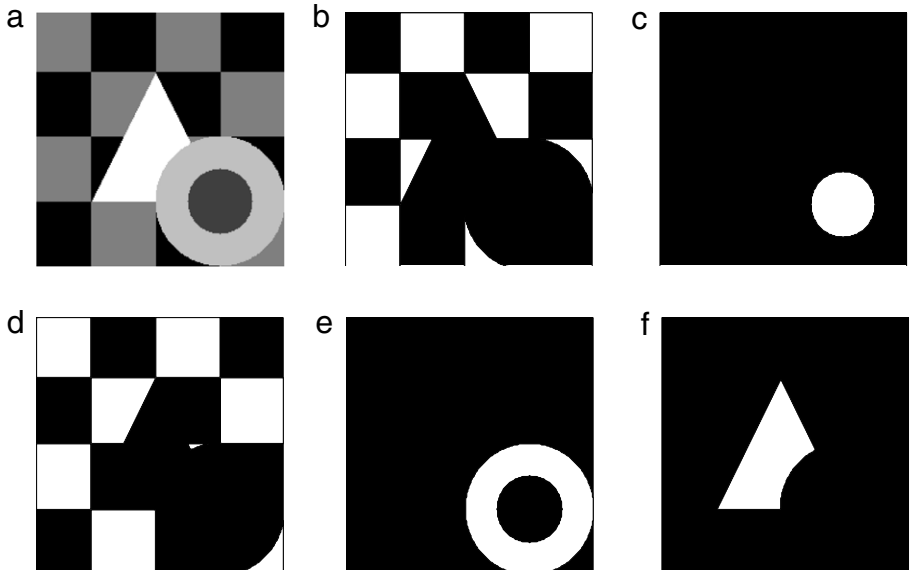

Fig. 6. A complex synthetic image with multiple objects and several generic visual structures. Image size is 256×256. (a) original image and (b)–(f) the filled contours for each level from $k = 0$ to $k = 4$.

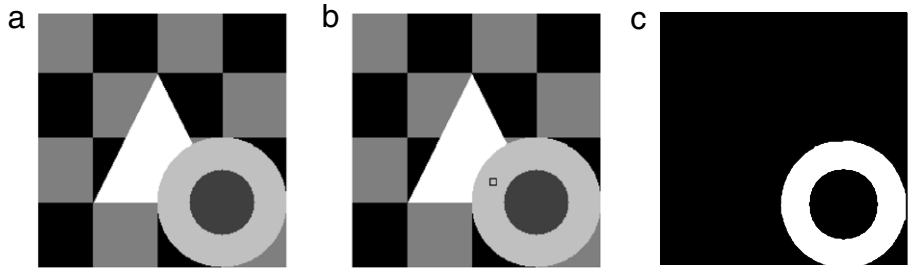

Fig. 7. A complex synthetic image with multiple objects and several generic visual structures (a) original image, (b) target image area, and (c) result.

handle such a case, we choose only one phase among multiple phases. Fig. 7 shows the application of the proposed model for segmenting the region of image which we are interested in. We get $B_2 = 0.2471$ and set $B_0 = 0, B_1 = B_0(1 - \text{tol}) + B_2\text{tol}$, $B_3 = B_2(1 - \text{tol}) + B_4\text{tol}$, and $B_4 = 1$. Here we take a specific tolerance, $\text{tol} = 0.5$, and the parameters ϵ_5, time step $\Delta t = 5\text{E} - 6$, $h = 1/256$, and $\lambda = 10$ are used. Fig. 8 shows the initialization with these values. This computation took 2 iterations and 0.625 s CPU time.

4.3. Synthetic image with noise

To show the efficiency of our proposed numerical scheme we choose a typical experiment from [7]. The example is a noisy synthetic image containing 4 stars on 4 different backgrounds (see Fig. 9(a) and (b)). Interface parameter ϵ_3, $\Delta t = 4\text{E} - 6$, $h = 1/128$, and $\lambda = 10$ are used with $B_0 = 0.0988, B_1 = 0.3281, B_2 = 0.5257, B_3 = 0.7190$, and

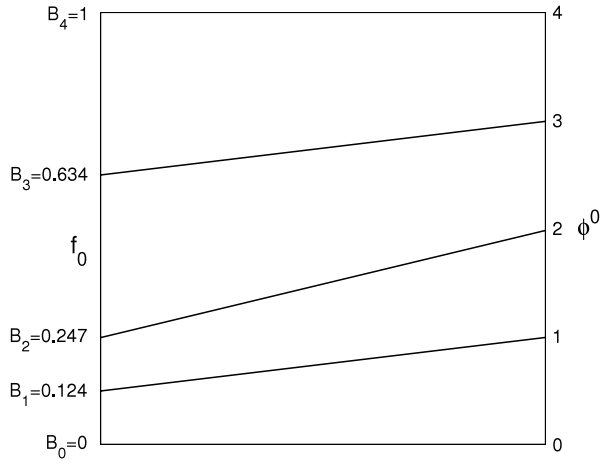

Fig. 8. Proposed initialization.

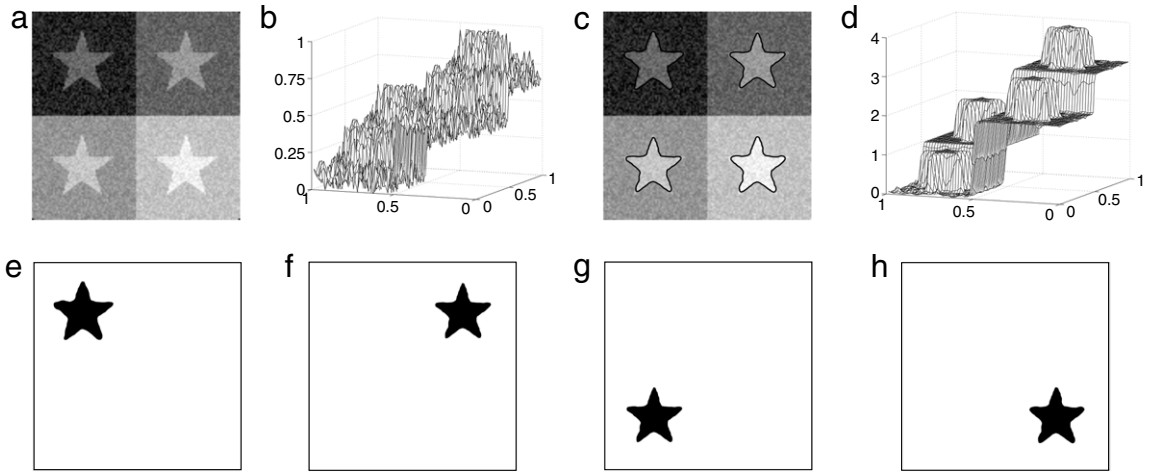

Fig. 9. (a) Original image f_0 with the size 256 × 256. (b) the value of original image f_0, (c) the final phase-field ϕ, (d) the value of the phase-field ϕ, and (e)–(h) the filled contours with $\phi = 0.5$, $\phi = 1.5$, $\phi = 2.5$, and $\phi = 3.5$, respectively.

$B_4 = 0.9209$. As can be seen, our method produces visually clear results with the five phase-fields after 15 iterations and 1.047 s CPU time.

4.4. Real landscape image

Fig. 10 shows the application of the proposed model to a real landscape image. The interface parameters ϵ_3, $\Delta t = 4\text{E} - 6$, $h = 1/128$, and $\lambda = 10$ are used with $B_0 = 0.1127$, $B_1 = 0.3146$, $B_2 = 0.4128$, $B_3 = 0.5264$, $B_4 = 0.7167$, and $B_5 = 0.9643$. Throughout this example, we show the final five segments detected by our proposed algorithm after 10 iterations and 0.797 s CPU time. (See Fig. 10(c) and (d).)

4.5. Brain MRI

Fig. 11 shows the application of the proposed model to a brain MRI segmentation with three levels. The interface parameter ϵ_2, $\Delta t = 5\text{E} - 6$, $h = 1/256$, and $\lambda = 10$ are used with $B_0 = 0.0348$, $B_1 = 0.4286$, and $B_2 = 0.8106$. We can see how the model can handle complex topologies. Fig. 11(a) is a brain MRI. Numerical results (b), (c), and (d) are filled contours at $\phi = 0$, 1, and 2, respectively. It only took 8 iterations and 1.735 s CPU time.

The final experiment shows the application of the proposed model for segmenting the selected region of image. Suppose that we only want to segment the gray part (small square box) in Fig. 12(a). We get the mean value inside the box as $B_2 = 0.4286$. Then set $B_0 = 0$, $B_1 = B_0(1 - \text{tol}) + B_2\text{tol}$, $B_3 = B_2(1 - \text{tol}) + B_4\text{tol}$, and $B_4 = 1$ with $\text{tol} = 0.75$. The gray area of brain is segmented with bright color as shown in Fig. 12(b) after 10 iterations and 2.187 s CPU time.

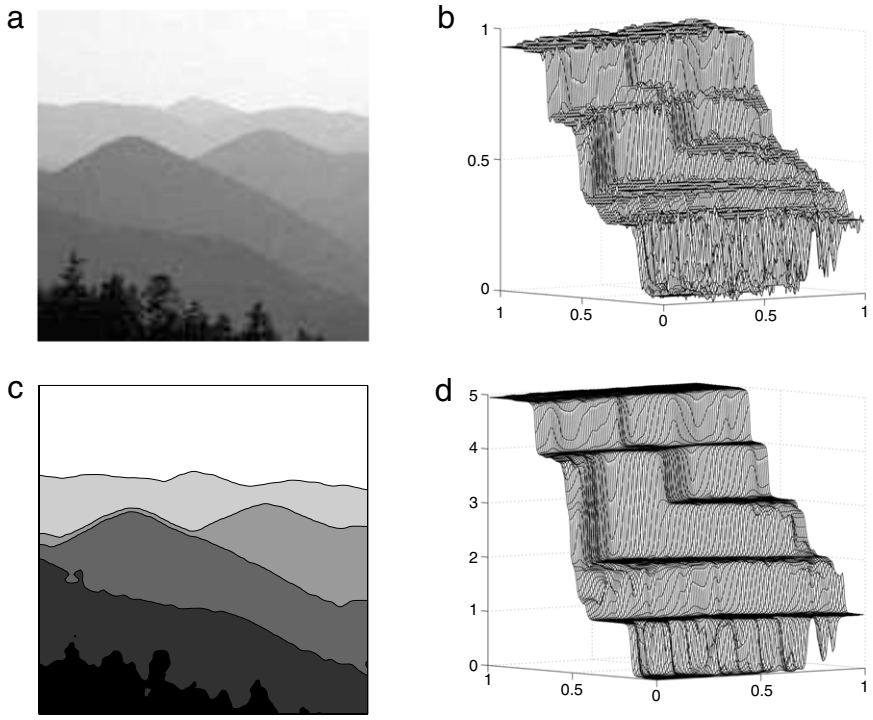

Fig. 10. Landscape image segmentation. Image size is 256 × 256. (a) Original image. (b) The value of original image. (c) Steady state filled contours. (d) The value of steady state.

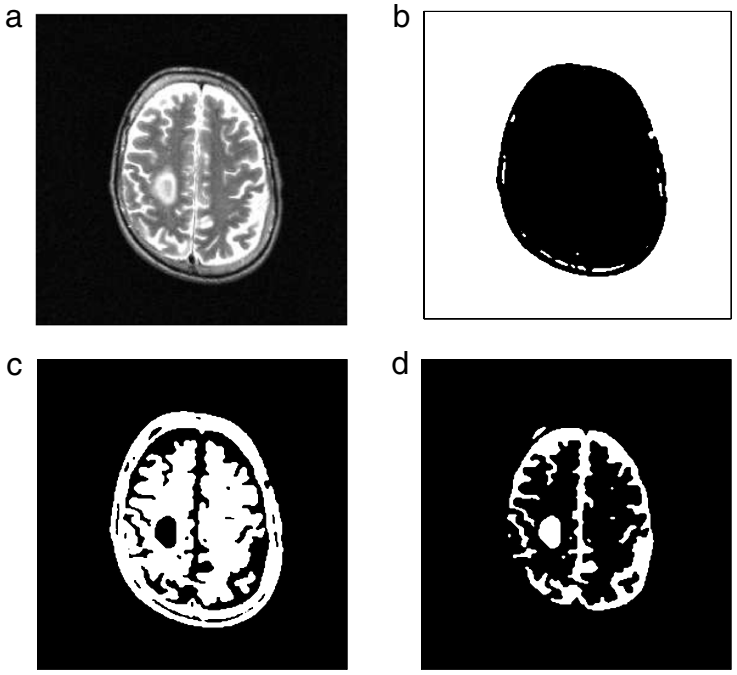

Fig. 11. Segmentation of a brain MRI using a three level phase-field. The size of the image is 256 × 256. (a) is a brain MRI. (b), (c), and (d) are filled contours at $\phi = 0$, 1, and 2, respectively.

5. Conclusion

Inspired by the multiphase image segmentation via Modica–Mortola phase transition we have proposed multiphase image segmentation using a phase-field model. We have shown that our proposed algorithm achieves faster segmentation

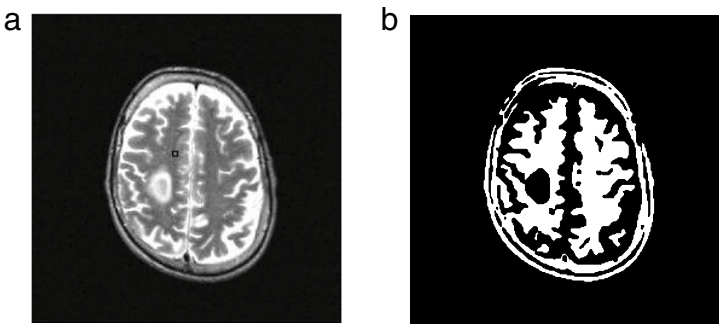

Fig. 12. Segmentation of a brain MRI using a three level phase-field. (a) is a brain MRI with a selected region, (b) is the segmentation result for the selected region.

of images than the previous method. We used a fast solver such as a multigrid method for solving the heat equation and an analytic solution for the nonlinear equation. We also propose an initialization algorithm based on the target objects for the fast image segmentation. We validated the proposed numerical method by various numerical results on artificial and real images.

Acknowledgments

This work was supported by the National Research Foundation of Korea(NRF) grant funded by the Korea government(MEST) (No. 2010-0027813). The authors also thank the anonymous referee for the constructive and helpful comments on the revision of this article.

References

[1] J.-M. Morel, S. Solimini, Variational Methods for Image Segmentation, Birkhäuser, 1994.
[2] T. Brox, J. Weickert, Level set segmentation with multiple regions, IEEE Trans. Image Process. 15 (10) (2006) 3213–3218.
[3] T.F. Chan, L.A. Vese, A multiphase level set framework for image segmentation using the Mumford and Shah model, Int. J. Comput. Vis. 50 (3) (2002) 271–293.
[4] G. Chung, L. Vese, Image segmentation using a multilayer level-set approach, Comput. Vis. Sci. 12 (2009) 267–285.
[5] L. He, S.J. Osher, Solving the Chan–Vese model by a multiphase level set algorithm based on the topological derivative, in: Proceedings of the 1st International Conference on Scale Space Variational Methods in Computer Vision, 2007, pp. 777–788.
[6] Y.M. Jung, S.H. Kang, J. Shen, Multiphase image segmentation via Modica–Mortola phase transition, SIAM J. Appl. Math. 67 (2007) 1213–1232.
[7] J. Lie, M. Lysaker, X.C. Tai, A variant of the level set method and applications to image segmentation, Math. Comp. 75 (2006) 1155–1174.
[8] F. Li, C. Shen, C. Li, Multiphase soft segmentation with total variation and $H1$ regularization, J. Math. Imaging Vision 37 (2010) 98–111.
[9] H. Li, X.C. Tai, Piecewise constant level set method for multiphase motion, Int. J. Numer. Anal. Model. 4 (2) (2007) 291–305.
[10] C. Samson, L. Blanc-Feraud, G. Aubert, J. Zerubia, A level set model for image classification, Int. J. Comput. Vis. 40 (3) (2000) 187–197.
[11] X.C. Tai, O. Christiansen, P. Lin, I. Skjaelaaen, Image segmentation using some piecewise constant level set methods with MBO type of project, Int. J. Comput. Vis. 73 (2007) 61–76.
[12] X.-F. Wang, D.-S. Huang, A novel multi-layer level set method for image segmentation, J. Univers. Comput. Sci. 14 (14) (2008) 2428–2452.
[13] S.M. Allen, J.W. Cahn, A microscopic theory for antiphase boundary motion and its application to antiphase domain coarsening, Acta Metall. 27 (1979) 1085–1095.
[14] Y. Li, H.G. Lee, D. Jeong, J.S. Kim, An unconditionally stable hybrid numerical method for solving the Allen–Cahn equation, Comput. Math. Appl. 60 (2010) 1591–1606.
[15] J.W. Cahn, On spinodal decomposition, Acta Metall. 9 (1961) 795–801.
[16] A. Karma, W.-J. Rappel, Quantitative phase-field modeling of dendritic growth in two and three dimensions, Phys. Rev. E 57 (1998) 4323–4349.
[17] J.C. Ramirez, C. Beckermann, A. Karma, H.-J. Diepers, Phase-field modeling of binary alloy solidification with coupled heat and solute diffusion, Phys. Rev. E 69 (2004) 051607.
[18] C.C. Chen, C.W. Lan, Efficient adaptive three-dimensional phase-field simulation of dendritic crystal growth from various supercoolings using rescaling, J. Cryst. Growth 311 (2009) 702–706.
[19] Y. Li, H.G. Lee, J.S. Kim, A fast, robust, and accurate operator splitting method for phase-field simulations of crystal growth, J. Cryst. Growth 321 (2011) 176–182.
[20] Q. Du, C. Liu, X. Wang, A phase field approach in the numerical study of the elastic bending energy for vesicle membranes, J. Comput. Phys. 198 (2004) 450–468.
[21] M. Bene, V. Chalupecky, K. Mikula, Geometrical image segmentation by the Allen–Cahn equation, Appl. Numer. Math. 51 (2004) 187–205.
[22] X. Feng, H.-J. Wu, A posteriori error estimates and an adaptive finite element method for the Allen–Cahn equation and the mean curvature flow, J. Sci. Comput. 24 (2005) 121–146.
[23] D. Jacqmin, Calculation of two-phase Navier–Stokes flows using phase-field modeling, J. Comput. Phys. 155 (1999) 96–127.
[24] J.S. Kim, A continuous surface tension force formulation for diffuse-interface models, J. Comput. Phys. 204 (2) (2005) 784–804.
[25] J.S. Kim, Phase field computations for ternary fluid flows, Comput. Methods Appl. Mech. Engrg. 196 (2007) 4779–4788.
[26] J.S. Kim, A generalized continuous surface tension force formulation for phase-field models for immiscible multi-component fluid flows, Comput. Methods Appl. Mech. Engrg. 198 (2009) 3105–3112.
[27] J. Shen, X. Yang, An efficient moving mesh spectral method for the phase-field model of two-phase flows, J. Comput. Phys. 228 (8) (2009) 2978–2992.
[28] X. Yang, J.J. Feng, C. Liu, J. Shen, Numerical simulations of jet pinching-off and drop formation using an energetic variational phase-field method, J. Comput. Phys. 218 (2006) 417–428.
[29] P.C. Fife, Models for phase separation and their mathematics, Electron. J. Differential Equations 2000 (48) (2000) 1–26.
[30] C. Cowan, M.S. Thesis, Simon Fraser University, Canada, 2005.
[31] W.L. Briggs, A Multigrid Tutorial, SIAM, Philadelphia, PA, 1987.
[32] U. Trottenberg, C. Oosterlee, A. Schüller, Multigrid, Academic Press, USA, 2001.
[33] A. Stuart, A.R. Humphries, Dynamical System and Numerical Analysis, Cambridge University Press, Cambridge, 1998.